Phonon dynamics of the Sn/Ge(111) surface at room temperature and low temperature determined by helium-atom scattering

J. Lobo,[1] D. Farías,[1,2] E. Hulpke,[3] and E. G. Michel[1,2]
[1]*Departamento de Física de la Materia Condensada, Universidad Autónoma de Madrid, 28049 Madrid, Spain*
[2]*Instituto Universitario de Ciencia de Materiales "Nicolás Cabrera," Universidad Autónoma de Madrid, 28049 Madrid, Spain*
[3]*Max-Planck-Institut für Strömungsforschung, Bunsenstr. 10, 37073 Göttingen, Germany*
(Received 3 January 2005; published 11 May 2005)

We report on a high-resolution helium atom scattering study of the surface lattice dynamics, for both the room temperature $(\sqrt{3}\times\sqrt{3})$R30° and the low-temperature (3×3) structures formed by 1/3 of a monolayer of Sn on Ge(111). At room temperature a pronounced lowering of the energy of the transversally polarized phonons along the $\overline{\Gamma\mathrm{M}}$ direction is observed for wave vectors in the vicinity of $Q=0.6$ Å^{-1}, the $\overline{\mathrm{K}}$ point of the room temperature $(\sqrt{3}\times\sqrt{3})$R30° structure. The temperature dependence of this mode is analyzed between 140 and 300 K. We conclude that the softening of this mode is related with the $(\sqrt{3}\times\sqrt{3})\mathrm{R30°}\leftrightarrow(3\times3)$ phase transition. Phonon distributions curves are determined for both phases and the two high symmetry directions. The experimental data are explained from the backfolding of the slightly modified Ge(111)-(1×1) Rayleigh wave and from the modes related to the Sn induced superstructures, in good agreement with first-principles calculations.

DOI: 10.1103/PhysRevB.71.205402 PACS number(s): 68.35.Ja, 68.35.Rh

I. INTRODUCTION

A lot of experimental and theoretical effort has been invested in studying phase transitions in low dimensional systems.[1] These systems provide insight into many fundamental problems in condensed matter physics.[1,2] The α phase of Sn/Ge(111) is obtained after depositing 1/3 of a monolayer (ML) of Sn onto Ge(111). α-Sn/Ge(111) exhibits a temperature-dependent phase transition from a $(\sqrt{3}\times\sqrt{3})$R30° structure at RT to (3×3) at low temperature (LT)[3] (see Fig. 1). Sn adatoms occupy in both phases T_4 coordination sites of the unreconstructed Ge(111) substrate.

Several different models have been put forward to explain the atomistic mechanism of the transition and the structural and electronic properties of the phases involved.[3–16] In particular, the surface charge density wave (SCDW) model[3] and the dynamical fluctuations model[4] have been frequently invoked to explain the experimental properties of these interfaces. The SCDW model is based on the observation of scanning tunneling microscopy (STM) images, where the (3×3) structure is interpreted in terms of a periodic charge redistribution, possibly accompanied by a small periodic lattice distortion, and stabilized by electron correlation effects.[3] Later on, the SCDW stabilization was related to the presence of surface defects creating local (3×3) patches.[13,14] These patches grow in size as temperature is lowered, finally covering the whole crystal surface.[13,14] The dynamical fluctuations model[4] sets out from the (3×3) structure, which is the stable configuration at ~100 K. The (3×3) reconstruction contains two different kinds of adsorbate atoms, with two different vertical heights.[4,5] At RT the (3×3) structure is maintained, but with a much smaller spatial correlation length, because the adatoms fluctuate rapidly (time scale of 1 ps) between the two vertical positions found in the (3×3) unit cell. These fluctuations become correlated and are greatly slowed down as temperature decreases, until eventually a (3×3) structure is observed in the surface. Thereby the local order is extended over the whole surface with larger correlated distances as the temperature is reduced. According to the dynamical fluctuations model the $(\sqrt{3}\times\sqrt{3})$R30° phase can be understood as the result of a vertical vibration of the (3×3) phase at RT. Since the vibration has a time scale of picoseconds (ps), it can only be monitored with faster techniques like photoemission[4,11] [STM is a slower technique, with response times of the order of milliseconds, while low-energy electron diffraction (LEED) needs long-range order]. From the structural point of view, surface x-ray diffraction (SXRD)[5,7,17] shows that the (3×3) phase is distorted along the surface normal. One out of the three adatoms that form the unit cell is displaced upwards, the other two inwards with a corrugation of ~0.3 Å. The structure of the $(\sqrt{3}\times\sqrt{3})$R30° phase is still controversial. Photoelectron diffraction (PED)[18,19] and x-ray standing wave (XSW) studies[9] favor the dynamical fluctuations model. SXRD studies at RT favor a flat Sn layer with all adatoms at the same height,[7] although a corrugated structure had also good agreement with the data.[8] The analysis the surface electronic structure and Sn core levels shows the existence of a split surface band and two components in the Sn core level, both at RT and LT. This similarity of both phases from the electronic point of view is also well explained by the dynamical fluctuations model.[4,11]

Theoretical calculations have proposed that a soft phonon might be behind the instability of a flat phase transition,[20] the driving force behind the instability of a flat $(\sqrt{3}\times\sqrt{3})$R30° structure. This mechanism has been experimentally confirmed using high-resolution helium atom scattering together with *ab initio* molecular dynamics calculations.[21] It has been shown that the high-temperature phase is a mixture of configurations with the same symmetry as the low-temperature state. Therefore, in spite of the fact that the driving force is a soft phonon, there is no ordered phase at high temperatures

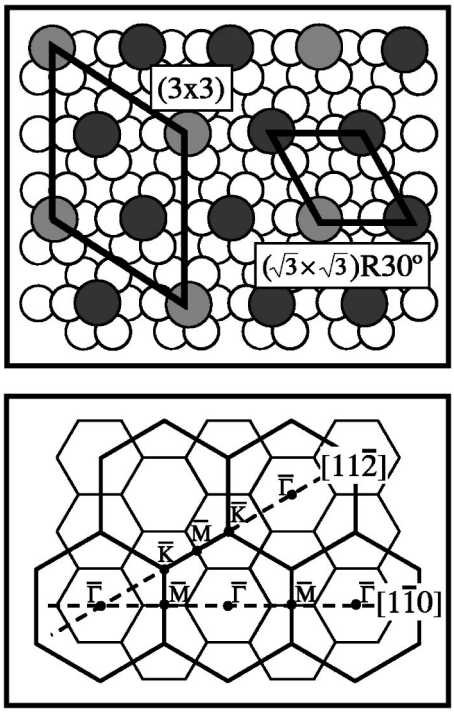

FIG. 1. Top: real space model of the $(\sqrt{3}\times\sqrt{3})$R30° and (3×3) structures of Sn/Ge(111), small open circles represent substrate atoms and large circles, Sn adatoms. If all Sn adatoms are equivalent, the surface displays a $(\sqrt{3}\times\sqrt{3})$R30° structure; if there is a height difference for the atoms marked by black and gray shadings, a (3×3) structure develops. Bold lines depict the respective unit cells. Bottom: reciprocal space and surface Brillouin zones for the $(\sqrt{3}\times\sqrt{3})$R30° (bold lines) and (3×3) (thin lines) structures. Labels of the high-symmetry points refer to the $(\sqrt{3}\times\sqrt{3})$R30° structure, high-symmetry directions are shown as dashed lines.

and the transition shows order-disorder character at room temperature and above.[9,21] These results show that the description of the surface phase transition of Sn on Ge(111) requires a careful analysis.[21]

In this paper, thermal helium scattering experimental results for both high-symmetry directions are analyzed. We present a description of the dynamics of both the $(\sqrt{3}\times\sqrt{3})$R30° and the (3×3) phases and show how they are modified along the phase transition. The results demonstrate the applicability of the above description of the phase transition. The contribution of the underlying Ge(111) is taken into account by an appropriate folding of the slightly modified Sn/Ge(111)-(1×1) Rayleigh wave (RW).

II. EXPERIMENT

The experiments are performed in a high-resolution helium-atom scattering (HAS) time-of-flight apparatus with a base pressure of 1.5×10^{-10} mbar. It features a fixed angle between the incident and the detected scattered beam of 101.8°. The incident beam of He is produced by means of an adiabatic expansion of the high pressure gas at 110 bar through a 10 μm aperture. The beam is subsequently chopped into short pulses before reaching the target chamber, to facilitate time-of-flight (TOF) analysis.[22] The total flight distance of the He particles from the target surface to the detector is 1.6985 m. By rotating the crystal around an axis normal to the sagittal plane, the incident beam angle is changed and different momentum transfers can be sampled. The velocity spread of the incident He beam ($\Delta v/v\sim1\%$, for beam energies in the range between 17.5 and 20 meV) is the main factor determining the experimental energy resolution, while the angular resolution is determined by the detector acceptance angle, which is about 0.2°.

The Ge(111) crystal was cut from a *n*-type polished commercial wafer ($\pm0.5°$, $\rho<0.4\ \Omega$ cm). Two molybdenum clips, serving as electrical contacts for resistive sample heating, were pressing it to a sapphire crystal which is mounted onto a high conductivity oxygen free Cu block. The six degrees of freedom of the manipulator allow for x, y, z linear movements as well as azimuthal, polar, and tilt rotations. Sample cooling is achieved through a high conductivity oxygen free Cu braid. Two thermocouples are used to monitor the temperature, one is attached to one of the Mo clips very close to the sample and the other one to the Cu block. The minimum sample temperature was 140 K.

The preparation of the Ge(111)-$c(2\times8)$ surface is performed using a procedure described previously.[23] The surface quality is checked from the high helium reflectivity (~30% at RT), the peaks sharpness in the helium diffraction patterns, and the ability to reproduce HAS spectra reported previously,[24] since these features are very sensitive to the presence of impurities.[25] The sample azimuth was aligned along the high-symmetry directions on the surface with the help of LEED and later by optimizing the HAS angular distributions.

Sn atoms were deposited using a Knudsen cell while heating the crystal to a temperature around ~500 K. During the deposition the pressure in the target chamber never exceeded 5×10^{-10} mbar. Throughout all the experiments the behavior of the evaporator turned out to be quite stable and reproducible. The flux of Sn atoms is calibrated accurately by monitoring the intensity of a 1/3 order diffraction peak along the $[1\bar{1}0]$ azimuth during the deposition. As shown in Fig. 2, this intensity exhibits a maximum at a coverage of 1/3 ML. Due to the low deposition rate used (1 ML/60 min), we estimate the calibration to be accurate to within ±0.01 ML,[25] defining 1 ML as the atomic density on the Ge(111) surface (7.21×10^{14} atoms/cm^2). The maximum of the 1/3 peak intensity in Fig. 2 is accompanied by a broad and shallow minimum in the specular peak intensity curve. The specular curve is too broad to be used for an equally accurate coverage determination.

The quality of the reconstructed Sn/Ge(111) surface was judged by examining the helium diffraction patterns along $[11\bar{2}]$ direction [$\overline{\Gamma K}$ of the $(\sqrt{3}\times\sqrt{3})$R30° phase] and $[1\bar{1}0]$ direction [$\overline{\Gamma M}$ of the $(\sqrt{3}\times\sqrt{3})$R30° phase]. These patterns are obtained by recording the scattered intensity on rotating the crystal about the polar angle. Typical angular distributions of this kind for both phases and the two high-symmetry directions are plotted in Fig. 3 which will be discussed in more detail in Sec. III. All these curves display sharp diffraction peaks. The full width at half maximum (FWHM) of the

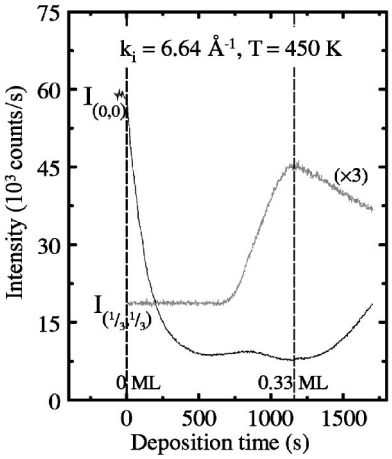

FIG. 2. Evolution of selected helium diffraction spot intensities during the deposition of Sn on Ge(111). The intensities of the specular beam (black line) and of the $(\frac{1}{3},\frac{1}{3})$ fractional order peak (gray line) along $[1\bar{1}0]$, are shown vs deposition time. The substrate temperature during the deposition was 450 K for an incoming He beam wave vector of 6.64 Å^{-1}.

specular peak (at $\Theta = 50.9°$) is ~0.15° which is similar to the acceptance angle of our detector. From this number the average terrace size can be estimated to be at least ~600 Å.[26] The widths of fractional order peaks coming from the $(\sqrt{3}\times\sqrt{3})$R30° structure does not change visibly with temperature, as shown for $[1\bar{1}0]$ direction in Fig. 3. The width is not

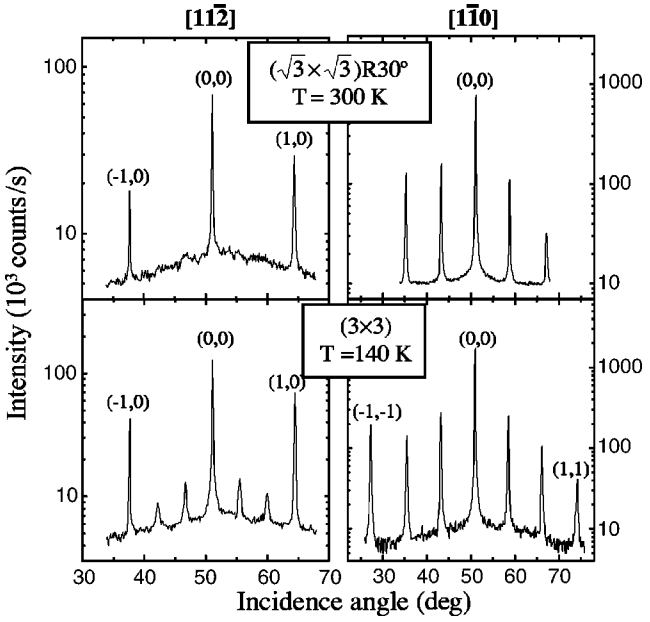

FIG. 3. Diffraction peaks in polar angle scans of the He beam intensity scattered from α-Ge(111) for an incoming wave vector of 6.58 Å^{-1}. The incoming angle is measured with respect to the surface normal. The two columns contain plots of data measured along the $[11\bar{2}]$ direction on the left and the $[1\bar{1}0]$ direction on the right. Top panels refer to the $(\sqrt{3}\times\sqrt{3})$R30° phase at RT and bottom panels to the (3×3) phase at 140 K. Note the disappearance of fractional order spots between LT and RT along $[11\bar{2}]$.

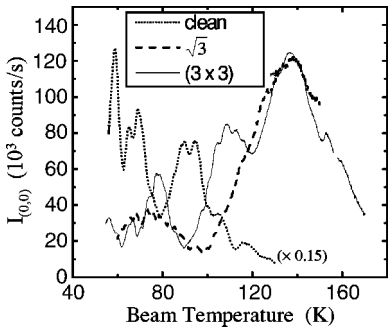

FIG. 4. Specular beam intensity as a function of nozzle temperature for helium scattering from Ge(111)-$c(2\times8)$ and the $(\sqrt{3}\times\sqrt{3})$R30° and (3×3) phases of α-Sn/Ge(111). The nozzle temperature determines the wave vector of the He atoms. Interference of beams reflected from terraces separated by steps as well as selective adsorption resonances are responsible for the different structures in these curves. The specular reflectivity of the clean surface is up to seven times larger than that of α-Sn/Ge(111).

much different for the (3×3) phase at LT. Thus, the average domain sizes are similar, with an estimated value of ~200 Å, indicating the formation of well-ordered surface structures.[25]

A significant thermal diffuse scattering is observed, supporting the existence of a certain amount of defects at the surface, in agreement with previous STM results.[13] Helium scattering is extremely sensitive to surface defects, and indeed the quasielastic peak dominates the TOF spectra (see also below).

III. RESULTS AND DISCUSSION

The evolution of the specularly reflected He signal as a function of nozzle temperature is measured for Ge(111)-$c(2\times8)$ and for the $(\sqrt{3}\times\sqrt{3})$R30° and (3×3) phases of α-Sn/Ge(111). Typical results of such "drift curves" along the $[11\bar{2}]$ azimuth are shown in Fig. 4. The incoming beam wave vector k_i is related to the nozzle temperature T_N by $k_i = \sqrt{5m\cdot k_B\cdot T_N}/\hbar$, where k_B is Boltzmann's constant, $\hbar$ is Planck's constant divided by 2π and m is the He atom mass. The structure observed in such curves is normally due to interference effects of He atoms scattered from terraces separated by steps of various heights. In this case, their shape is influenced also by selective adsorption resonances, which originate from resonant transitions of the incoming He atoms into bound states of the He-surface interaction potential well.[25] These drift curves were used to choose the optimum parameters for the experiments. Phonon inelastic measurements are best performed at outgoing angles close to the specular peak. Therefore the scattering conditions are chosen such that the specular intensity is maximum. For the Sn/Ge(111) surface this happens at a nozzle temperature of 138 K corresponding to $k_i = 7.54$ Å^{-1} ($E_i = 29.7$ meV). The angular distributions shown in Fig. 3 were measured for a slightly different incoming wave vector, $k_i = 6.58$ Å^{-1} ($E_i = 22.6$ meV). This value corresponds to a nozzle temperature of 105 K where the (3×3) phase drift curve displays a local maximum.

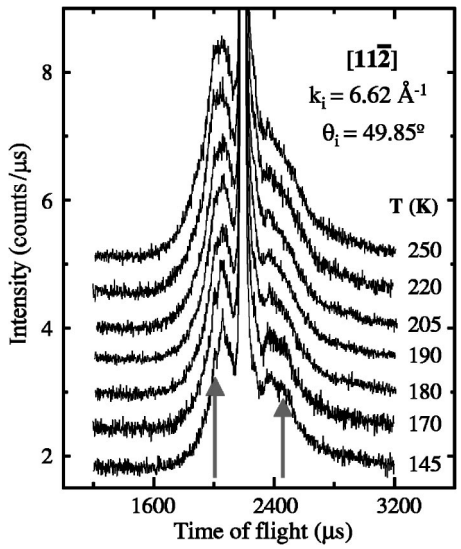

FIG. 5. TOF spectra as a function of surface temperature. The data were taken along the $[11\bar{2}]$ direction at an angle of incidence of 49.85° and with helium wave vector of $k_i = 6.62$ Å^{-1}. Curves in this plot are displaced for clarity, labels on the intensity scale refer to the spectrum at $T = 145$ K. The largest peak, due to diffuse elastic scattering, is truncated. Its maximum intensity amounts ~45 cps/μs. Each TOF spectrum has been integrated over 10 h. Peaks related to the (3×3) phase and modified along the phase transition are marked by arrows.

Figure 3 shows helium diffraction patterns along the two high-symmetry surface directions for α-Sn/Ge(111) above (RT) and below (140 K) the transition temperature, which have been briefly discussed before. Integer order peaks correspond to the unreconstructed Ge(111) surface. The same periodicity is observed in the HAS angular distributions recorded along $[1\bar{1}0]$ at LT and RT, while along the $[11\bar{2}]$ azimuth all fractional third order peaks disappear at RT. The relative intensity between the specular and the fractional peaks along $[1\bar{1}0]$ does not change as temperature is lowered. This indicates that the corrugation amplitudes of both the $(\sqrt{3}\times\sqrt{3})$R30° and (3×3) phases are similar, in agreement with previous findings.[16]

TOF spectra were measured for different scattering conditions to determine the low-energy vibrations of α-Sn/Ge(111). In this way, the surface phonon dispersion curves for the LT (3×3) and the RT $(\sqrt{3}\times\sqrt{3})$R30° phases are obtained along the two high-symmetry directions.[27]

Figure 5 presents a series of TOF spectra measured along the $[11\bar{2}]$ direction as a function of surface temperatures and for the same scattering conditions. Up to five inelastic peaks are resolved in the spectra. The diffuse elastic peak at 2205 μs is truncated by a factor of five and dominates all the inelastic features. The large intensity of the diffuse elastic peak indicates the presence of defects at the surface. Their density can be estimated from the spectra shown as $\lesssim$5%. On the other hand, the low intensity of the inelastic features made it necessary to employ long measuring times (4–10 h for each TOF spectrum) in order to achieve sufficiently good statistics in the rather weak inelastic peaks. The intensity of the phonon inelastic peaks depends on the surface temperature T. Indeed, they are a sensitive fingerprint reflecting the dynamical changes of the surface across the phase transition. Some peaks (e.g., the ones at 2005 and 2435 μs, marked by arrows) disappear above the critical temperature (T_c). The value of T_c is ~190 K, and it is estimated from a careful monitoring of the temperature dependence of the inelastic peaks. This value is to be compared to previously found values: 215 K (see Ref. 3), ~70 K (see Ref. 12), 180 K (for domains of 200 Å), and 217 K (for domains of 400 Å).[16] The broad range of critical temperatures found (~120 K) can be explained from the existence at the surface of a certain concentration of hopping defects. A detailed analysis is presented elsewhere.[28]

Typical TOF results are shown in Fig. 6. All TOF spectra in these plots are converted to an energy transfer scale. Data for the two reconstructions and the two high-symmetry directions are shown (see caption for details). Again, the large truncated peak in the energy transfer spectra is due to diffuse elastic scattering from defects and is about five times more intense than the other peaks, which present clearly resolved single phonon inelastic events. When comparing the TOF spectra obtained for the $(\sqrt{3}\times\sqrt{3})$R30° phase along both high-symmetry directions, we find that the peaks along $[1\bar{1}0]$ are more intense and clearly resolved than those along $[11\bar{2}]$, even though in some cases the integration time for the latter ones amounted up to 10 h. In the spectra for the (3×3) phase all peaks are clearly resolved in both high-symmetry directions.

The positions of individual peaks in the above energy transfer spectra and the transferred parallel momenta (according to the incident angles) provide data points for the surface phonon dispersion curves. Such data are shown in Fig. 7 for the $(\sqrt{3}\times\sqrt{3})$R30° phase and in Fig. 8 for the (3×3) phase.

A first approach to explain the form and position of the different branches of the surface phonon dispersion curves shown in Figs. 7 and 8 is to interpret them in terms of backfolding of the RW of the unreconstructed Ge(111) surface covered with 1/3 ML of Sn [subsequently called (1×1)-RW], which involves the reciprocal lattice vectors $\mathbf{G}_{m,n}$ of the respective structures. To this end, the dispersion curve of the (1×1)-RW is assumed to be given by a formula similar to the one successfully used for Si(111)-(7×7) (see Ref. 29) and for Ge(111)-$c(2\times8)$ (see Ref. 23):

$$\Delta E(\mathbf{Q}) = \left\{ \sum_{i=1}^{2} [C_1 \sin^2(\mathbf{A}_i \cdot \mathbf{Q}) + C_2 \sin^2(2\mathbf{A}_i \cdot \mathbf{Q}) + C_3 \sin^4(2\mathbf{A}_i \cdot \mathbf{Q})] \right\}^{1/2}, \quad (1)$$

where ΔE denotes the phonon energy in meV and $\mathbf{Q}$ is the phonon wave vector in Å^{-1}, $\mathbf{A}_1 = a/2[10\bar{1}]$ and $\mathbf{A}_2 = a/2[\bar{1}10]$ are vectors oriented along close packed rows in the surface ($a = 5.66$ Å is the Ge lattice constant) and C_i are parameters adjustable to fit the data. The backfolding is

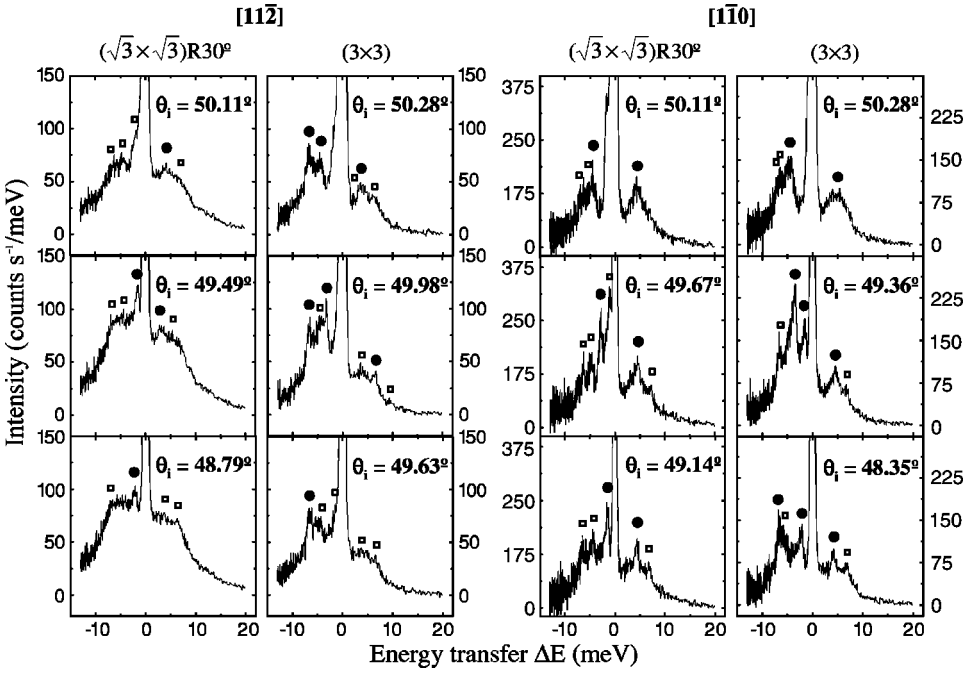

FIG. 6. Phonon inelastic peaks in evaluated TOF spectra obtained by He scattering from α-Sn/Ge(111) for a variety of different incoming angles θ_i, along the two high-symmetry directions, and for two different surface temperatures. The measured spectra are converted to an energy-transfer scale, where the different values of θ_i determine different amounts of parallel momentum transferred to the surface. The spectra are grouped according to experimental conditions. Columns 1 (RT) and 2 [140 K, (3×3)] present measurements along $[11\bar{2}]$ with a He beam energy of 29.7 meV (k_i=7.54 Å^{-1}). Columns 3 (RT) and 4 [140 K, (3×3)] present measurements along $[1\bar{1}0]$, with a He beam energy of 22.6 meV (k_i=6.58 Å^{-1}). Two types of symbols mark single phonon inelastic peaks: filled circles correspond to intense and well-resolved features and open squares to weaker ones.

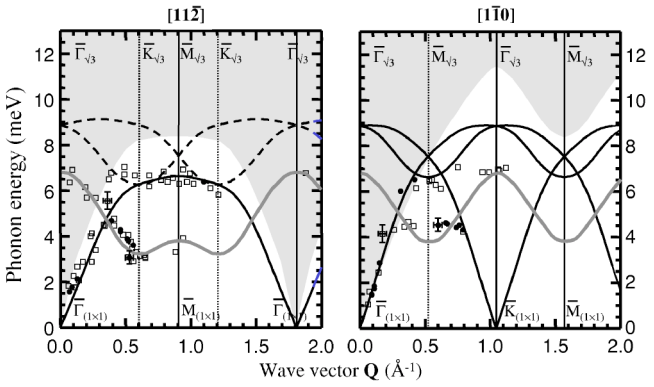

FIG. 7. Surface phonon dispersion curves for Sn/Ge(111)-$(\sqrt{3}\times\sqrt{3})$R30° in an extended-zone scheme along the $[11\bar{2}]$ direction (left) and the $[1\bar{1}0]$ direction (right). Data points are obtained from all the TOF spectra measured and the different symbols refer to strong (filled circles) and weak (open squares) features in these spectra (see Fig. 6). Shaded areas are projections of the Ge bulk modes onto the (111) surface, bold black lines correspond to the Rayleigh wave, according to Eq. (1), lines correspond to backfolding by in-plane $\mathbf{G}_{m,n}$ reciprocal vectors (solid lines), and to out-of-plane reciprocal vectors of the superstructure (broken lines). Gray lines are calculated dispersion curves from Ref. 21. Also shown are the Brillouin zone boundaries of the (1×1) and the $(\sqrt{3}\times\sqrt{3})$R30° structure as solid and dotted vertical lines, respectively.

achieved by replacing **Q** by $\frac{1}{2}(\mathbf{K}-\mathbf{G}_{m,n})$ where **K** is the desired surface phonon wave vector for the reconstructed surface and $\mathbf{G}_{m,n}$ are reciprocal lattice vectors of the respective phases, $\mathbf{G}_{(\sqrt{3}\times\sqrt{3})\mathrm{R30°}}$ for the $(\sqrt{3}\times\sqrt{3})$R30° and $\mathbf{G}_{(3\times3)}$ for the (3×3) phase.

Best fits to all the data in Figs. 7 and 8 were obtained for C_1=44 meV^2, C_2=4 meV^2, and C_3=6 meV^2. For comparison, the values obtained for the clean Ge(111) surface are

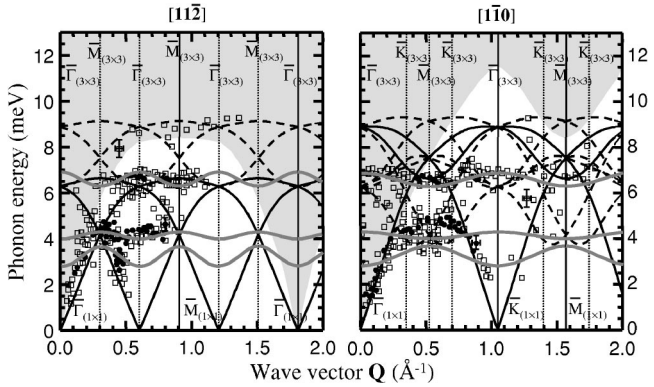

FIG. 8. Surface phonon dispersion curves for α-Sn/Ge(111)-(3×3) in an extended-zone scheme along the $[11\bar{2}]$ direction (left) and the $[1\bar{1}0]$ direction (right). Data points, shaded areas and the different types of lines are described in Fig. 7.

C_1=61 meV^2, C_2=6 meV^2, and C_3=2 meV^2 (Ref. 23). The resulting dispersion curves for the RW are shown as solid black lines in Figs. 7 and 8. Not all the data are fit by these curves. A first, minor effect is that the reconstruction itself causes a distortion of the curves.[30] The main reason is the appearance of additional modes[21] and the formation of gaps at the Brillouin zone boundaries,[31] which are not accounted for in this approach.

The modes related directly to the surface reconstruction have been calculated previously.[21] Two approaches were used. In the first one, plane-wave generalized gradient approximation in the density functional theory is used to calculate the frequencies for the $\bar{\Gamma}$ point. In the second, the frequencies are obtained by fitting an up to second-nearest-neighbor coupling model to the experimental phonon frequencies. We compare now these calculations with experimental data along both $[1\bar{1}0]$ and $[11\bar{2}]$ directions. The calculated modes from Ref. 21 are represented as gray lines in Figs. 7 and 8. The minimum in the dispersion curve along $[11\bar{2}]$ at $\bar{K}_{\sqrt{3}}$ occurs at Q=0.60 Å^{-1}, precisely the critical wave vector value of the soft phonon associated with the phase transition predicted in the work of Pérez *et al.*[20]

Almost all the experimental points of the dispersion curves in Figs. 7 and 8 are explained by either the backfolded RW or by the calculated modes. The good agreement is enhanced when data and calculated curves are plotted in the reduced Brillouin zones of the respective structural phases, as done in Fig. 9. In the case of the $(\sqrt{3}\times\sqrt{3})$R30° phase, the extra points of the surface modes are well reproduced along all the Brillouin zone. For the (3×3) phase, the backfolded points give rise to several bands, broadened by the experimental error and the superposition due to the backfolding. The bands are well reproduced, either by the RW folding or by the calculated bands. Note that along the $[11\bar{2}]$ direction the most intense peaks correspond to the surface modes, reproduced by the calculations. The small size of the (3×3) Brillouin zone compared to that of bulk terminated Ge(111) requires a very high resolution in the wave vector scale in order to be sensitive to changes. The resolution in the present studies is on the order of $\delta|\Delta\mathbf{K}|/|\mathbf{k}_i|\simeq10^{-3}$, with $\Delta\mathbf{K}$ denoting the parallel momentum transfer to the surface and $\mathbf{k}_i$ the wave vector of the incoming He atoms.

Temperature dependent structural phase transitions are frequently classified analyzing the order of the two phases involved. There are two limiting cases corresponding to displacive and order-disorder transitions.[32,33] In displacive transitions the system evolves from a state with long-range order to another ordered state as the critical temperature is crossed. The LT state displays a lower symmetry. In order-disorder transitions, on the other hand, the ordered state at LT becomes disordered at high temperatures, and this high-temperature state has, averaged over time, again a higher symmetry. This simple classification might be helpful, but real phase transitions usually exhibit a more complex behavior. Indeed, the distinction between displacive or order-disorder behavior is difficult if the accessible temperature range is not large enough. This is frequently the case when only a narrow range around the critical temperature is probed. We refer the reader to Refs. 34–37 for more detailed treatments.

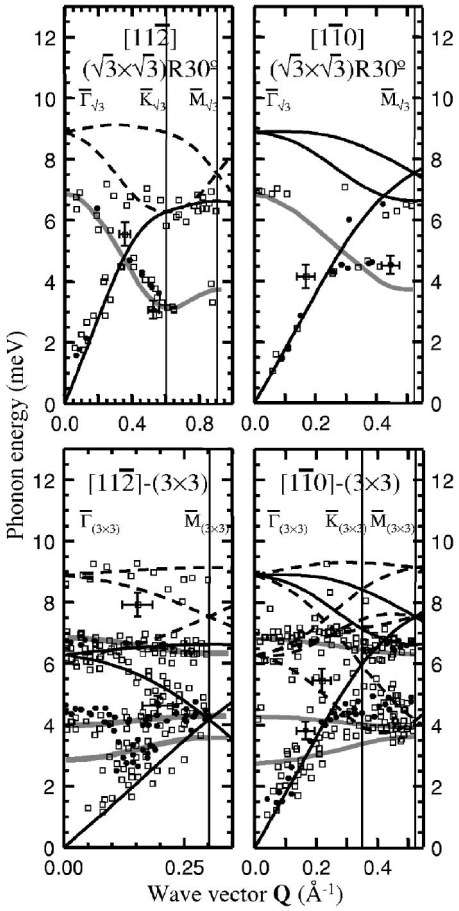

FIG. 9. Surface phonon dispersion data for the $(\sqrt{3}\times\sqrt{3})$R30° phase (top panels) and the (3×3) phase (bottom panels) in a reduced-zone scheme along the $[11\bar{2}]$ direction (left) and the $[1\bar{1}0]$ direction (right). Data points and the different types of lines as in Fig. 7.

Displacive transitions are commonly associated to a soft phonon, i.e., an optic frequency which tends to zero at the phase transition. The displacement pattern of the soft phonon determines the structure of the LT phase in a displacive transition. This description of the origin of the atomic displacements in a displacive transition is easy to understand and it is commonly employed. However, we recall that there is no known system where this simple picture is fulfilled. As stated above, a purely displacive behavior is a limiting case. In real systems, the dynamics of the order parameter is more complex than expected for a purely displacive system, and the soft mode frequency never goes to zero, but remains finite at the phase transition point. Furthermore, the softening is usually accompanied by the so called "central peak," a modification of the low frequency distribution.[38]

In the case of two dimensional systems, there are only few experimental observations of soft modes. We restrict ourselves to structural phase transitions on a surface, where the simultaneous softening of a phonon mode is observed. The most important examples are W(100),[34] H/W(110),[39] and H/Mo(110).[40] In all these cases there is a more or less

pronounced decrease of the energy of a phonon mode at the phase transition. All of them have in common that the polarization of the soft phonon is longitudinal. We note that for Sn/Ge(111) the phase transition is driven by the softening of a transverse vibrational mode.[21] There has been a long-standing polemics on the nature of the $\sqrt{3}$ phase, specially because in some early studies it was described as a "flat" adlayer of atoms, while the (3×3) phase would be slightly corrugated. This is the scenario of a phase transition which would be fairly well described by a simple displacive model. Different structural and electronic studies support that in the $\sqrt{3}$ phase Sn atoms vibrate vertically around (3×3) equilibrium positions.[8] This phase is not flat, unless observed with a technique much slower than the vibration frequency, as the STM. It rather corresponds to a (3×3) phase without long range order. This picture describes well the behavior in a fairly broad temperature range, from the critical temperature up to at least 500 K,[18] and it is well reproduced by molecular dynamics simulations.[21] The resulting dynamics of the phase transition has been described before.[21] It is in agreement with the experiments, and it reflects a more complex pattern than the simplest displacive or order-disorder transitions.

IV. CONCLUSIONS

High-resolution HAS are used to study the surface lattice dynamics of the room temperature $(\sqrt{3}\times\sqrt{3})$R30° and the low temperature (3×3) phases of α-Sn/Ge(111). The surface phonon dispersion curves for both phases and high-symmetry directions are determined. Experimental results are well reproduced either by backfolding the Rayleigh wave of the Ge(111) surface, or by specific surface modes. The description of the phase transition agrees with the predictions of the dynamical fluctuations model.

ACKNOWLEDGMENTS

We are grateful to Professor J. P. Toennies for the critical reading of the manuscript and his hospitality in Göttingen. We also thank A. Cano and Professor A. P. Levanyuk for fruitful discussions. This work has been supported by Ministerio de Ciencia y Tecnología (Spain) (Grant No. BFM-2001-0244), by Comunidad de Madrid (Grant No. 07N/0022/2002), the "Programa Ramón y Cajal" (Ministerio de Ciencia y Tecnología), and by the Max-Planck-Gesellschaft (Germany).

[1] B. N. J. Persson, Surf. Sci. Rep. **15**, 1 (1992).
[2] A. Mascaraque and E. G. Michel, J. Phys.: Condens. Matter **14**, 6005 (2002).
[3] J. M. Carpinelli, H. H. Weitering, M. Bartkowiak, R. Stumpf, and E. W. Plummer, Phys. Rev. Lett. **79**, 2859 (1997).
[4] J. Avila, A. Mascaraque, E. G. Michel, M. C. Asensio, G. LeLay, J. Ortega, R. Pérez, and F. Flores, Phys. Rev. Lett. **82**, 442 (1999).
[5] A. Mascaraque, J. Avila, J. Alvarez, M. C. Asensio, S. Ferrer, and E. G. Michel, Phys. Rev. Lett. **82**, 2524 (1999).
[6] J. Ortega, R. Pérez, and F. Flores, J. Phys.: Condens. Matter **12**, L21 (2000).
[7] O. Bunk, J. H. Zeysing, G. Falkenberg, R. L. Johnson, M. Nielsen, M. M. Nielsen, and R. Feidenhansl, Phys. Rev. Lett. **83**, 2226 (1999).
[8] SXRD data favor a flat $\sqrt{3}$ structure, but the χ^2 difference with respect to a distorted structure is very small.[7]
[9] J. S. Okasinski, C. Y. Kim, D. A. Walko, and M. J. Bedzyk, Phys. Rev. B **69**, 041401(R) (2004).
[10] T. E. Kidd, T. Miller, M. Y. Chou, and T. C. Chiang, Phys. Rev. Lett. **85**, 3684 (2000).
[11] R. I. G. Uhrberg and T. Balasubramanian, Phys. Rev. Lett. **81**, 2108 (1998).
[12] A. V. Melechko, M. V. Simkin, N. F. Samatova, J. Braun, and E. W. Plummer, Phys. Rev. B **64**, 235424 (2001).
[13] A. V. Melechko, J. Braun, H. H. Weitering, and E. W. Plummer, Phys. Rev. B **61**, 2235 (2000).
[14] H. H. Weitering, J. M. Carpinelli, A. V. Melechko, and Jiandi Zhang, Science **285**, 2107 (1999).
[15] G. Ballabio, S. Scandolo, and E. Tosatti, Phys. Rev. B **61**, R13345 (2000); G. Ballabio, G. Profeta, S. deGironcoli, S. Scandolo, G. E. Santoro, and E. Tosatti, Phys. Rev. Lett. **89**, 126803 (2002).
[16] L. Floreano, D. Cvetko, G. Bavdek, M. Benes, and A. Morgante, Phys. Rev. B **64**, 075405 (2001).
[17] J. Zhang, Ismail, P. J. Rous, A. P. Baddorf, and E. W. Plummer, Phys. Rev. B **60**, 2860 (1999).
[18] L. Petaccia, L. Floreano, A. Goldoni, D. Cvetko, A. Morgante, L. Grill, A. Verdini, G. Comelli, G. Paolucci, and S. Modesti, Phys. Rev. B **64**, 193410 (2001).
[19] L. Petaccia, L. Floreano, M. Benes, D. Cvetko, A. Goldoni, L. Grill, A. Morgante, A. Verdini, and S. Modesti, Phys. Rev. B **63**, 115406 (2001).
[20] R. Pérez, J. Ortega, and F. Flores, Phys. Rev. Lett. **86**, 4891 (2001).
[21] D. Farías, W. Kamiński, J. Lobo, J. Ortega, E. Hulpke, R. Pérez, F. Flores, and E. G. Michel, Phys. Rev. Lett. **91**, 016103 (2003).
[22] G. Brusdeylins, R. B. Doak, and J. P. Toennies, Phys. Rev. B **27**, 3662 (1983).
[23] J. Lobo, D. Farías, E. Hulpke, J. P. Toennies, and E. G. Michel (unpublished).
[24] D. Farías, G. Lange, K. H. Rieder, and J. P. Toennies, Phys. Rev. B **55**, 7023 (1997).
[25] D. Farías and K. H. Rieder, Rep. Prog. Phys. **61**, 1575 (1998).
[26] G. Comsa, Surf. Sci. **81**, 57 (1979).
[27] The transfer of parallel momentum to the surface is varied in these experiments by changing the incident angle and the He beam energy. In the case of the $(\sqrt{3}\times\sqrt{3})$R30° phase, the incident angle θ_i was varied between 47.1° and 51.3° along the $[11\bar{2}]$ and between 48.7° and 52.9° along the $[1\bar{1}0]$ direction. For the (3×3) phase θ_i values between 48.3° and 53.8° were chosen along the $[11\bar{2}]$ and between 44.2° and 53.0° along the $[1\bar{1}0]$ direction.

[28] A. Cano, A. P. Levanyuk, and E. G. Michel, Nanotechnology **16**, 325 (2005).
[29] G. Lange, J. P. Toennies, P. Ruggerone, and G. Benedek, Europhys. Lett. **41**, 647 (1998).
[30] P. Santini, L. Miglio, G. Benedek, and P. Ruggerone, Surf. Sci. **241**, 346 (1991).
[31] L. Miglio, P. Santini, P. Ruggerone, and G. Benedek, Phys. Rev. Lett. **62**, 3070 (1989).
[32] B. A. Strukov and A. P. Levanyuk, *Ferroelectric Phenomena in Crystals* (Springer-Verlag, Berlin, 1998).
[33] A. D. Bruce and R. A. Cowley, Adv. Phys. **29**, 219 (1980).
[34] H. J. Ernst, E. Hulpke, and J. P. Toennies, Phys. Rev. B **46**, 16 081 (1992).
[35] T. Schneider and F. Stoll, Phys. Rev. B **13**, 1216 (1976).
[36] A. D. Bruce, K. A. Muller, and W. Berlinger, Phys. Rev. Lett. **42**, 185 (1979).
[37] T. Schneider and E. Stoll, Ferroelectrics **24**, 67 (1980).
[38] V. Ginzburg, A. Levanyuk, and A. Sobyanin, Phys. Rep. **57**, 151 (1980).
[39] E. Hulpke and J. Lüdecke, Phys. Rev. Lett. **68**, 2846 (1992).
[40] E. Hulpke and J. Lüdecke, Surf. Sci. **287-288**, 837 (1993).